HHS Public Access

Author manuscript

J Med Chem. Author manuscript; available in PMC 2025 April 14.

Published in final edited form as:

J Med Chem. 2025 February 13; 68(3): 3433–3444. doi:10.1021/acs.jmedchem.4c02646.

Discovery of Orally Available Prodrugs of Itaconate and Derivatives

Chae Bin Lee[††],
Johns Hopkins Drug Discovery, Johns Hopkins School of Medicine, Baltimore, Maryland 21205, United States

Ivan Šnajdr[††],
Institute of Organic Chemistry and Biochemistry, Academy of Sciences of the Czech Republic v.v.i., Prague 160 00, Czech Republic

Lukáš Tenora,
Johns Hopkins Drug Discovery, Johns Hopkins School of Medicine, Baltimore, Maryland 21205, United States; Institute of Organic Chemistry and Biochemistry, Academy of Sciences of the Czech Republic v.v.i., Prague 160 00, Czech Republic

Jesse Alt,
Johns Hopkins Drug Discovery, Johns Hopkins School of Medicine, Baltimore, Maryland 21205, United States

Sadakatali Gori,
Johns Hopkins Drug Discovery, Johns Hopkins School of Medicine, Baltimore, Maryland 21205, United States

Marcela Krečmerová,
Institute of Organic Chemistry and Biochemistry, Academy of Sciences of the Czech Republic v.v.i., Prague 160 00, Czech Republic

R. Michael Maragakis,
Johns Hopkins Drug Discovery, Johns Hopkins School of Medicine, Baltimore, Maryland 21205, United States

James Paule,

Corresponding Authors Pavel Majer – majer@uochb.cas.cz, **Barbara S. Slusher** – bslusher@jhmi.edu, **Rana Rais** – rrais2@jhmi.edu.
[††]C.B.L. and I.Š. contributed equally to this work.

ASSOCIATED CONTENT

Supporting Information

The Supporting Information is available free of charge at https://pubs.acs.org/doi/10.1021/acs.jmedchem.4c02646.

^{1}H and ^{13}C (APT) NMR spectra and LC-MS chromatogram and spectra for prodrugs **P1–P15;** molecular formula strings and the associated biochemical and biological data (PDF)

SMILES, permeability data, mouse plasma and skin stability, human plasma and skin stability for prodrugs **P1–P15**, IA, 1-MI, 4-MI, DMI, 4-OI (CSV)

Complete contact information is available at: https://pubs.acs.org/10.1021/acs.jmedchem.4c02646

The authors declare the following competing financial interest(s): L.T., I.S., M.K., L.G., P.M., B.S.S., and R.R. are inventors on Johns Hopkins University (JHU) patents covering novel compositions of itaconate prodrugs and their utility. These patents have been licensed to Sun Pharma Advanced Research Company Ltd. (SPARC). This arrangement has been reviewed and approved by the JHU in accordance with its conflict-of-interest policies. Other authors declare that no conflicts of interest exist.

Johns Hopkins Drug Discovery, Johns Hopkins School of Medicine, Baltimore, Maryland 21205, United States

Sandhya Tiwari,
In Vitro Biology, Sun Pharma Advanced Research Company Ltd., Vadodara 391775 Gujarat, India

Jitesh Iyer,
In Vitro Biology, Sun Pharma Advanced Research Company Ltd., Vadodara 391775 Gujarat, India

Rashmi Talwar,
In Vitro Biology, Sun Pharma Advanced Research Company Ltd., Vadodara 391775 Gujarat, India

Luis Garza,
Department of Dermatology, Johns Hopkins University School of Medicine, Baltimore, Maryland 21205, United States

Pavel Majer,
Institute of Organic Chemistry and Biochemistry, Academy of Sciences of the Czech Republic v.v.i., Prague 160 00, Czech Republic

Barbara S. Slusher,
Johns Hopkins Drug Discovery, Departments of Neurology, Psychiatry and Behavioral Sciences, Neuroscience, Medicine, Oncology, and Department of Pharmacology and Molecular Sciences, Johns Hopkins School of Medicine, Baltimore, Maryland 21205, United States

Rana Rais
Johns Hopkins Drug Discovery, Departments of Neurology, and Department of Pharmacology and Molecular Sciences, Johns Hopkins School of Medicine, Baltimore, Maryland 21205, United States

Abstract

Itaconate, an endogenous immunomodulator from the tricarboxylic acid (TCA) cycle, shows therapeutic effects in various disease models, but is highly polar with poor cellular permeability. We previously reported a novel, topical itaconate derivative, SCD-153, for the treatment of alopecia areata. Here, we present the discovery of orally available itaconate derivatives for systemic and skin disorders. Four sets of prodrugs were synthesized using pivaloyloxymethyl (POM), isopropyloxycarbonyloxymethyl (POC), (5-methyl-2-oxo-1,3-dioxol-4-yl) methyl (ODOL), and 3-(hexadecyloxy)propyl (HDP) pro-moieties pairing with itaconic acid (IA), 1-methyl itaconate (1-MI), and 4-methyl itaconate (4-MI). Among these, POC-based prodrugs (**P2, P9, P13**) showed favorable stability, permeability, and pharmacokinetics. Notably, **P2** and **P13** significantly inhibited Poly(I:C)/IFNγ-induced inflammatory cytokines in human epidermal keratinocytes. Oral studies demonstrated favorable pharmacokinetics releasing micromolar concentrations of IA or 4-MI from **P2** and **P13**, respectively. These findings highlight the potential of prodrug strategies to enhance itaconate's cellular permeability and oral bioavailability, paving the way for clinical translation.

Graphical Abstract

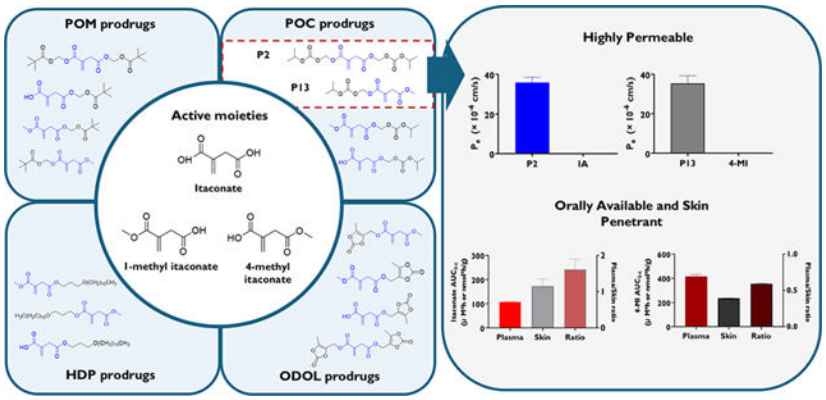

INTRODUCTION

Itaconic acid (IA, itaconate) is an endogenous immunomodulatory metabolite produced by diverting aconitate from the tricarboxylic acid (TCA) cycle during the activation of inflammatory macrophages. IA is an unsaturated dicarboxylic acid synthesized by immune-responsive gene 1 (IRG1).[1] IA acts on multiple inflammatory pathways and is shown to be an essential functional component of activated macrophages.[2,3] Despite being a widely used commercial biomaterial derived from Aspergillus for decades, its identification as a mammalian immunometabolite was not established until 2011.[2,4] It acts as an immunomodulator through several mechanisms: inhibition of succinate dehydrogenase (SDH),[5] activation of Nrf2 via alkylation of KEAP1,[6] regulation of ATF3/IκBζ inflammatory axis,[7] inhibition of glycolysis,[5] regulation of type I IFNs[8] and inhibition of NLRP3 inflammasome.[9]

Itaconate contains an α,β-unsaturated alkene and shares structural similarity with other metabolites like phosphoenolpyruvate, succinate, malonate, and fumarate. There is a growing body of evidence suggesting that itaconate, as well as its derivatives, have promise in various disease models.[6,10] Despite promising efficacy in preclinical models, clinical potential of IA is limited due to its highly polar structure, making it impermeable to biological membranes. Several cell-permeable itaconate analogs, including dimethyl itaconate (DMI), 4-octyl itaconate (4-OI), and 4-ethyl itaconate (4-EI) have been developed to mimic the actions of endogenous itaconate. DMI and 4-OI, interestingly have been shown to conserve the anti-inflammatory effects of IA[11,12] but fall short in their ability to convert to intracellular IA once delivered.[8,13] Additionally, it has been reported that DMI is intracellularly converted into a mixture of 1-methyl itaconate (1-MI) and 4-methyl itaconate (4-MI) and presumably exerts its effects through these active metabolites, rather than itaconate itself.[13]

The immunomodulatory properties of itaconate and its derivatives make them promising pharmacologic candidates for treating inflammatory conditions such as psoriasis, rheumatoid arthritis, systemic lupus erythematosus, and multiple sclerosis.[1,14,15] We have recently designed and reported a topical, cell-permeable prodrug of 4-MI, termed SCD-153

as a novel treatment for alopecia areata,[16] which is a chronic autoimmune disorder characterized by the targeted destruction of hair follicles by CD8+ T cells, leading to hair loss. Interestingly, topical administration of SCD-153 to C57BL/6 mice resulted in a significant increase in hair growth, exhibiting statistically superior effects compared to the vehicle (dimethyl sulfoxide), less cell-permeable itaconate analogues (4-MI and DMI), as well as the clinically used JAK inhibitor tofacitinib. SCD-153 demonstrated considerable skin concentrations, indicating that the prodrug strategy has promise in topically delivering IA to previously impermeable tissues.[16]

Building on the initial strategy, this work aimed to develop orally available, cell-permeable prodrugs of IA or its monoesters, 1-MI and 4-MI, to target tissues such as skin systemically. We employed FDA-approved promoieties such as pivaloyloxymethyl (POM), isopropyloxycarbonyloxymethyl (POC), (5-methyl-2-oxo-1,3-dioxol-4-yl) methyl (ODOL) and 3-(hexadecyloxy)-propyl (HDP) to mask either the 1-carboxylate or 4-carboxylate on itaconate, thereby enhancing its permeability and pharmacokinetic properties.

CHEMISTRY

The synthesis of IA prodrugs focused on three structural types: (a) itaconate diesters with identical ester groups, (b) itaconate monoesters with ester groups at the 4-position of the carboxylate, and (c) itaconate diesters derived from 1-methyl or 4-methyl itaconate, featuring various promoieties at the second carboxylic function. The prodrug groups utilized were FDA approved promoieties, including pivaloyloxymethyl (POM), isopropyloxycarbonyloxymethyl (POC), (5-methyl-2-oxo-1,3-dioxol-4-yl)methyl (ODOL), and 3-(hexadecyloxy)-propyl (HDP) to minimize challenges related to translation and toxicity.[17–19] For example, these groups were applied in the prodrug development of acyclic nucleoside phosphonates, including Adefovir, Tenofovir, and Cidofovir which led to substantial improvement in pharmacokinetics and oral absorption.[20,21] We have also reported their application in successfully synthesizing prodrugs of the multiply charged GCPII inhibitor 2-(phosphonomethyl)pentanedioic acid (2-PMPA) and demonstrated enhancement in oral bioavailability (20–69 fold) in mice and dogs.[22,23]

Synthesis of itaconate diesters bis-POM (**P1**), bis-POC (**P2**), and bis-ODOL (**P3**) were performed by alkylation of IA with carbonyloxymethyl chlorides or (5-methyl-2-oxo-1,3-dioxol-4-yl)methyl chloride, respectively, under basic conditions in the presence of sodium iodide (Scheme 1).

Selective monoesterification of free IA to POM, POC, or ODOL was challenging; various reaction conditions were attempted, but only a nonseparable mixture of 1- and 4-monoesters were obtained. Thus, to synthesize pure 4-monoesters with a free 1-carboxylate, 4-*tert*-butyl itaconate (**5**) was prepared according to a published protocol[24] and alkylation was performed under the same conditions as described above. The protected diesters **6–8** were subsequently treated with trifluoroacetic acid to give the desired monoesters **P4, P5**, and **P6** (Scheme 2). Preparation of 3-(hexadecyloxy)propyl monoester (**P7**) was achieved by reaction of itaconic anhydride (**9**) with hexadecyloxypropanol (**10**) at 70 °C in chloroform proceeding selectively to the position 4 (Scheme 2).

Mixed diesters **P8–15** were prepared by alkylation of 1-MI (**11**) or 4-MI (**12**) with a chloromethyl derivative (analogously as described for compounds **P1–3**) or by Steglich esterification with 3-(hexadecyloxy)propanol (compounds **P11** and **P15**, Scheme 3).

RESULTS AND DISCUSSION

In Vitro Chemical Stability, Permeability, and Metabolic Stability Assessments.

To develop orally available prodrugs for IA, 1-MI, and 4-MI, it was crucial to achieve high permeability, good chemical stability, and the ability to release active compounds upon oral absorption. Consequently, the prodrugs were assessed for their chemical stability under gastrointestinal pH conditions (1.2, 4.5, and 7.4) to ensure stability in the gut for oral delivery. Those demonstrating good pH stability were further evaluated for their ability to permeate via the parallel artificial membrane permeation assay (PAMPA, GIT) assay.[25] Finally, stable and highly permeable prodrugs were assessed for stability in mouse and human plasma, as well as in skin homogenates to assess release of actives at the desired site, as detailed in Table 1 below.

All prodrugs were either highly stable (>80% remaining at 1 h) or moderately stable (50–80% remaining at 1 h) across the three pH conditions, with the exception of POM, POC, and ODOL monoesters of IA (**P4, P5**, and **P6** respectively), which all exhibited complete instability at pH 7.4.

The calculated *c* log *P* values of the prodrugs expectedly showed significant improvement in lipophilicity, approximately 10-fold for POC and POM, and 50-fold for HDP prodrugs, compared to their respective active moieties (*c* log *P*: −0.33, 0.14, and 0.20 for IA, 4-MI, and 1-MI, respectively) (SwissADME, Lausanne, Switzerland).[26] Given the polar nature of the ODOL promoieties, its addition did not enhance itaconate calculated lipophilicity. In terms of permeability via PAMPA-GIT assay to mimic permeability via the gastrointestinal tract, bis-POM and bis-POC-protected IA prodrugs (**P1, P2**), as well as POM/POC prodrugs of 1-MI (**P8, P9**) and 4-MI (**P12, P13**), demonstrated excellent in vitro permeability with a permeation index (P_e) greater than 10×10^{-6} cm/s. These results are consistent with the increase in their *c* log *P*, aligning with previous studies showing that permeability increases with lipophilicity when cLogP values are 3.5 or lower.[27] Conversely, POM or POC monoesters of IA (**P4, P5**), as expected, displayed poor permeability, with a P_e values less than 1×10^{-6} cm/s, due to the retain charged site on one terminus. Regarding the ODOL prodrugs, the trend was similar, with the bis-ODOL ester of IA (P3) and ODOL-esters of 1-MI (**P10**) and 4-MI (**P14**) demonstrating high permeability, while the monoester of IA (**P6**) demonstrating limited permeability. Overall, all ODOL prodrugs (**P3, P6, P10**, and **P14**) exhibited a significant enhancement in the permeability ($P_e \sim 15 \times 10^{-6}$ cm/s) of both IA and 4-MI. These results align with previously reported ODOL-based prodrugs, such as azilsartan medoxomil, faropenem medoxomil and 2-PMPA-tetraODOL, which demonstrated significantly enhanced oral bioavailability.[22,28,29] However, in the case of itaconate and analogs ODOL promoiety did not outperform POM and POC based prodrugs in enhancing permeability attributed to the highly polar surface area of the ODOL promoiety. Consequently, ODOL prodrugs were not further advanced into pharmacokinetic studies.

Interestingly, all HDP prodrugs displayed poor permeability ($P_e < 1 \times 10^{-6}$ cm/s) except for the IA monoester HDP prodrug (**P7**) which had a slightly better, but comparably lower permeability, ($P_e = 3.21 \times 10^{-6}$ cm/s) to POM and POC analogs. This poor permeability was attributed to their exceptionally high lipophilicity, with *c* log *P* values exceeding 5 for **P7, P11**, and **P15** (*c* log *P*: 8.38, 8.79, and 8.91, respectively). Such high *c* log *P* values are also associated with poor solubility, reflecting an unfavorable hydrophilic–lipophilic balance and resulting in suboptimal properties.[30] These findings suggest that, overall, HDP prodrugs were not effective candidates for improving the oral bioavailability of IA analogs.

To evaluate the potential for oral delivery of active compounds to systemic circulation in inflammatory conditions and to ensure skin targeting in the in vivo PK study, we focused on mouse and human plasma and skin homogenates. These models were selected because they closely mimic the enzymatic and metabolic environments of the in vivo matrices under investigation. However, as most of these compounds are ester-based prodrugs, we anticipate that other highly metabolic organs, such as the liver, may also play a significant role in their metabolic pathways, although this was not tested in the current study.

All POC, POM and ODOL prodrugs except the monoesters of IA (**P4** and **P5**) were found to hydrolyze in mouse and human plasma readily. However, the monoesters of IA were chemically unstable, and showed poor permeability (Table 1) and therefore were not selected for further consideration. HDP prodrugs, interestingly, showed stability in both mouse and human plasma. However, when incubated in mouse skin homogenate, the HDP-based prodrugs were unstable (<50% remaining at 1 h). In human skin homogenate, POM and POC-based prodrugs demonstrated instability similar to mouse skin homogenate. Interestingly, ODOL-based prodrugs, except the bis-ODOL prodrug (**P3**), had moderate stability (>50% remaining after 1h) while HDP-based prodrugs were completely stable in human skin homogenates (>90% remaining at 1 h).

Collectively, POM (**P1, P8** and **P12**) and POC (**P2, P9** and **P13**) based prodrugs showed the most promise, with enhanced PAMPA permeability and effective release of active moieties in plasma and skin. While the POM-based prodrugs showed comparable stability and permeability results, the well-known additional toxicity attributed to POM promoieties due to carnitine depletion[31] led us to advance the three POC-based prodrugs **P2** (IA), **P9** (1-MI) and **P13** (4-MI) for in vitro gene expression efficacy studies, and in vivo mouse pharmacokinetic evaluation as described below.

Immunomodulatory Effects of P2, P9 and P13 in Stimulated Human Epidermal Keratinocytes.

We theorized that itaconate-based cell permeable prodrugs may offer benefits for alopecia areata (as we have previously shown) by counteracting immune stimulants such as Poly(I:C) and IFNγ as these stimulants have shown to contribute to the disease by activating the NLRP3 inflammasome activity[32,33] and JAK-STAT signaling.[34–37] IA and its derivatives have been shown to suppress proinflammatory cytokines such as IL-6, a JAK-STAT activator, and IL-1β, which disrupts hair cycling and is elevated in alopecia areata scalp lesions.[38–41] Thus, to validate the therapeutic potential of **P2, P9** and **P13**, we evaluated their dose-dependent cytotoxicity and ability to block Poly(I:C) and IFNγ-induced cytokines

and chemokines release in vitro in normal human epidermal keratinocytes (NHEKs) as previously described (Figure 1).[16] First, the in vitro cytotoxicity of the prodrugs was assessed to ensure they did not adversely affect cell viability. After 8 h of treatment, NHEKs treated with **P2, P9**, and **P13** all demonstrated good cell viability, with over 80% of cells remaining viable at the highest concentration of 100 μM (data not shown). The immunomodulatory effects were next evaluated by adding **P2, P9** and **P13** to NHEKs stimulated with Poly(I:C) or IFNγ to induce IL-6, IL-1β, IFNβ, and IFN-inducible chemokines (CXCL9, CXCL10, CXCL11), which are recognized as characteristic markers of alopecia areata.[42] For IFNγ-inducible chemokines (CXCL9, CXCL10, and CXCL11), **P2** and **P13** showed significant effects, with over 50% inhibition at 30–100 μM. However, **P9** exhibited limited inhibitory effects, with less than 50% inhibition at 100 μM. This suggests that although the IA- and 4-MI-releasing prodrugs were effective, the 1-MI-releasing prodrug was less so, indicating that the free carboxylate at the 1-position on IA is essential for activity, and masking it resulted in a decrease in effectiveness. Similarly, IL-1β although showed low induction (2–3 fold) when stimulated with Poly(I:C) + IFNγ, **P2** and **P13** demonstrated over 50% inhibition of this signal at concentrations ≥10 μM, and **P9** showed effects at 100 μM. **P2** and **P13** also showed significant, dose-dependent inhibition of IL-6 and **P2** in addition showed dose dependent inhibition of IFNβ, while **P9** did not, further suggesting that IA or 4-MI are more active versus 1-MI in this assay.

Overall, among POC-based prodrugs, **P2** and **P13** showed significantly enhanced immunomodulatory effects in NHEKs, supporting our hypothesis that cell permeable prodrugs may offer benefits for alopecia areata. This was further evidenced in our screening data in NHEKs, where neither 4-MI nor 1A affected the mRNA expression of TLR3 (Toll-like receptor 3) and IL-6 involved in inflammatory response while the prodrugs **P2** and **P13** caused >90% inhibition (Figure S1).

Pharmacokinetic Studies in Mice.

Given their promising immunomodulatory effects in NHEKs, we next conducted pharmacokinetic evaluation of P2 and P13 at a dose of 100 mg/kg equivalent in mice. The dose was selected based on previously reported dose of 25–150 mg/kg[43–45] and to achieve effective concentrations (30–100 μM) in in vitro NHEK model.

The concentration–time profiles of released IA from **P2** and released 4-MI from **P13** in plasma and skin are presented in Figure 2. Following oral administration, intact **P2** was not detectable in the plasma, suggesting rapid hydrolysis of **P2** into IA. The C_{max} of released IA in plasma following **P2** administration (100 mg/kg IA equivalent) was 83.8 ± 18.8 μM, observed at 15 min postdose (T_{max}), as shown in Figure 2C. The C_{max} of IA in skin was 65.9 ± 10.2 nmol/g. Notably, **P2** showed significant distribution to skin tissue, indicated by higher skin versus plasma AUC_{0-t} values (173 ± 30.0 nmol·h/g and 108 ± 2.68 μM·h, respectively), resulting in a skin/plasma ratio of 1.61 ± 0.29. The half-life of itaconate released from **P2** was calculated to be 1.42 ± 0.24 h in plasma and 3.32 ± 1.23 h in skin, demonstrating longer retention and slower clearance from the skin compared to plasma.

Similarly, following oral administration of **P13** (100 mg/kg eq of 4-MI), intact **P13** was undetectable in plasma, indicating that **P13** was rapidly hydrolyzed into 4-MI. The released 4-MI showed high exposure in plasma, with a C_{max} of 349 ± 39.3 μM and an AUC_{0-t} of 415 ± 16.8 μM·h. 4-MI released from **P13** also exhibited high exposure in skin tissue, with an AUC_{0-t} value of 234 ± 1.30 nmol·h/g. The skin/plasma ratio of 4-MI after **P13** administration was calculated to be 0.59 ± 0.01. The half-life of 4-MI released from **P13** was calculated to be 0.87 ± 0.09 h in plasma and 0.97 ± 0.20 h in skin. Overall, its exposure in the skin exceeded 100 μM, a concentration that resulted in over 50% inhibition of cytokines in NHEKs (Figure 1).

Collectively, **P2** and **P13** demonstrated efficient delivery of active moieties to systemic circulation and skin. While comparative PK data for IA and 4-MI versus their prodrugs are lacking in this study, our results clearly support the prodrug strategy. IA and 4-MI showed poor permeability in the PAMPA assay (Table 1), failed to inhibit cytokine production in NHEKs (Figure S1), and 4-MI was ineffective in vivo in the alopecia areata model, unlike **P13** when compared at equimolar doses.[16] These findings highlight the limitations of the parent compounds and underscore the potential of prodrugs like **P2** and **P13** to overcome these challenges, aligning with prior literature on the importance of enhancing cellular permeability for itaconate derivatives.[13,14,46,47]

Another limitation of this study is the absence of direct comparisons between our prodrugs and traditional treatments for alopecia areata, such as JAK inhibitors. Although future studies could address this gap, in our previous work, topical application of 5% **P13** using an alternate-day, two-dose regimen significantly promoted hair growth compared to 5% tofacitinib under the same conditions[16] Moreover, while JAK inhibitors like tofacitinib are effective, they carry risks of serious adverse effects, including venous thromboembolism and other on-target toxicities.[48,49] In contrast, itaconate prodrugs act through a distinct mechanism, reducing the likelihood of such on-target side effects. In support, we assessed **P13'**s preliminary toxicity profile (given its robust efficacy in alopecia areata) at two doses via systemic administration. No hematological changes or weight loss were observed (Figure S2 and Table S1), supporting the safety of **P13**. These findings suggest that itaconate prodrugs offer a promising, potentially safer alternative for treating alopecia areata.

CONCLUSIONS

In summary, we synthesized four sets of IA, 4-MI, and 1-MI prodrugs using the FDA-approved promoieties POM, POC, ODOL, and HDP by incorporating itaconate diester, itaconate monoester, and itaconate diesters derived from monomethyl itaconate. These prodrugs were evaluated in a panel of in vitro and pharmacokinetic assays. The POC-based prodrugs of IA (**P2**) and 4-MI (**P13**) demonstrated the best properties including chemical stability in gastric conditions, high permeability, release of the active moiety in skin homogenates, and positive immunomodulatory effects in NHEK assays. **P2** and **P13** also exhibited good pharmacokinetic properties following oral administration. The ability of these prodrugs to effectively deliver the active IA and 4-MI to skin tissue following oral administration, suggests that they hold potential as oral treatments for alopecia areata and other inflammatory skin diseases.

EXPERIMENTAL SECTION

Chemicals and Materials.

A commercially available reagent or HPLC-grade solvents and materials were used for the synthesis of the compounds described. All chemicals were reagent grade purchased from Sigma-Aldrich, Combi-Blocks, or Tokyo Chemical Industry (TCI) Co. Ltd. TLC was performed on Silica gel 60 F254-coated aluminum sheets (Merck) and spots were visualized with UV light and by the solution of $Ce(SO_4)_2{\cdot}4H_2O$ (1%) and $H_3P(Mo_3O_{10})_4$ (2%) in sulfuric acid (10%). Column chromatography was performed on silica gel 60 (0.063–0.200 mm, Fluorochem). NMR spectra were measured on Bruker AVANCE 400 instrument. ^1H NMR was recorded at 401 MHz, and signals of TMS (δ 0.0, $CDCl_3$) and $CDCl_3$ (δ 7.26) were used for standardization. ^{13}C NMR spectra were recorded at 101 MHz, and the signal of $CDCl_3$ (δ 77.16) was used for standardization. The chemical shifts are given in δ scale; the coupling constants J are given in Hz. The low-resolution ESI mass spectra were recorded using a ZQ micromass mass spectrometer (Waters). High-resolution ESI mass spectra were recorded using an LTQ Orbitrap XL spectrometer (Thermo Fisher Scientific). The purity of all compounds subjected to biological testing was over 95%.

General Synthetic Procedure for Prodrugs P1–3.

IA (200 mg, 1.53 mmol, 1 equiv), appropriate chloride 2–4 (2.5–3 equiv), sodium iodide (46.1 mg, 0.307 mmol, 0.2 equiv), and potassium carbonate (3–4 equiv) were dissolved in anhydrous MeCN (5–10 mL) and the mixture was stirred for 16 h at 45–55 °C under inert atmosphere. EtOAc (60 mL) was added, and the mixture was washed with brine (20 mL) and sat. Sodium thiosulfate (10 mL). The organic phase was dried over anhydrous Na_2SO_4, volatiles were evaporated, and the residue was purified by flash column chromatography on silica (various mobile phases) to afford compounds P1–3.

Bis((pivaloyloxy)methyl) 2-Methylenesuccinate (P1).—Chloromethyl pivalate (**2**) (579 mg, 554 μL, 3.84 mmol, 2.5 equiv); potassium carbonate (637 mg, 4.61 mmol, 3 equiv); MeCN (5 mL); 45 °C; mobile phase: cyclohexane/EtOAc, 5:1. Compound P1 was isolated as a colorless oil (199 mg) in 36% yield. **^{1}H NMR** (401 MHz, $CDCl_3$): δ_H 1.20 (s, 18H), 3.38 (d, J = 1.0 Hz, 2H), 5.74 (s, 2H), 5.82 (s, 3H), 6.41 (s, 1H). **^{13}C NMR** (101 MHz, $CDCl_3$): δC 26.83, 26.84, 37.12, 38.75, 38.78, 79.70, 79.82, 130.52, 132.33, 164.45, 169.12, 177.07. **ESI MS:** 381.2 ($[M + Na]^+$). **HRMS (ESI):** calcd. For $C_{17}H_{26}O_8Na$ 381.15199, found: 381.15158.

Bis(((isopropoxycarbonyl)oxy)methyl) 2-Methylenesuccinate (P2).—Chloromethyl isopropyl carbonate (3) (586 mg, 514 μL, 3.84 mmol, 2.5 equiv); potassium carbonate (637 mg, 4.61 mmol, 3 equiv); MeCN (5 mL); 45 °C; mobile phase: cyclohexane/EtOAc, 5:1. Compound **P2** was isolated as a colorless oil (79.2 mg) in 14% yield. **^{1}H NMR** (401 MHz, $CDCl_3$): δ_H 1.30 (s, 6H), 1.31 (s, 6H), 3.41 (s, 2H), 4.82–4.98 (m, 2H), 5.75 (s, 2H), 5.82 (s, 2H), 5.85 (s, 1H), 6.46 (s, 1H). **^{13}C NMR** (101 MHz, $CDCl_3$): δ_C 21.63, 36.95, 73.13, 82.00, 82.22, 131.05, 131.99, 153.26, 153.29, 164.28, 168.95. **ESI MS:** 385.1 ($[M + Na]^+$). **HRMS (ESI):** calcd. For $C_{15}H_{22}O_{10}Na$ 385.11052, found: 385.11069.

Bis((5-methyl-2-oxo-1,3-dioxol-4-yl)methyl) 2-Methylenesuccinate (P3).—(4-Chloromethyl)-5-methyl-1,3-dioxol-2-one (**4**) (685 mg, 504 μL, 4.61 mmol, 3 equiv); potassium carbonate (850 mg, 6.15 mmol, 4 equiv); MeCN (10 mL); 55 °C; mobile phase: cyclohexane/EtOAc, 1:1. Compound **P3** was isolated as a colorless oil (311 mg) in 57% yield. **^{1}H NMR** (401 MHz, $CDCl_3$): δ_H 2.17 (s, 3H), 2.19 (s, 3H), 3.38 (d, J = 1.1 Hz, 2H), 4.86 (s, 2H), 4.92 (s, 2H), 5.81 (s, 1H), 6.40 (s, 1H). **^{13}C NMR** (101 MHz, $CDCl_3$): δ_C 9.48, 9.52, 37.57, 54.39, 54.50, 130.62, 132.59, 133.32, 133.34, 140.45, 140.49, 152.22, 165.41, 170.05. **ESI MS:** 279.0 ($[M + Na]^+$). **HRMS (ESI):** calcd. For $C_{11}H_{12}O_7Na$ 279.04752, found: 279.04800.

General Synthetic Procedure for Compounds 6–8.

3-(*tert*-Butoxycarbonyl)but-3-enoic acid (**5**) (400 mg, 2.15 mmol, 1 equiv), appropriate chloride **2–4** (1.2–1.3 equiv), sodium iodide (64.4 mg, 0.430 mmol, 0.2 equiv) and potassium carbonate (445 mg, 3.22 mmol, 1.5 equiv) were dissolved in anhydrous MeCN (5 mL) and the mixture was stirred for 16 h at 45–55 °C. EtOAc (60 mL) was added, and the mixture was washed with brine (20 mL) and sat. Sodium thiosulfate (10 mL). The organic phase was dried over anhydrous Na_2SO_4, volatiles were evaporated, and the residue was purified by flash column chromatography on silica (various mobile phases) to afford desired compounds **6–8** as colorless oils.

1-(tert-Butyl) 4-((Pivaloyloxy)methyl) 2-Methylenesuccinate (6).—Chloromethyl pivalate (**2**) (421 mg, 402 μL, 2.79 mmol, 1.3 equiv); 45 °C; mobile phase: cyclohexane/EtOAc, 6:1. Compound **6** was isolated as a colorless oil (458 mg) in 71% yield. **^{1}H NMR** (401 MHz, $CDCl_3$): δ_H 1.21 (s, 9H), 1.48 (s, 9H), 3.33 (d, J = 1.2 Hz, 2H), 5.63 (d, J = 1.2 Hz, 1H), 5.76 (s, 2H), 6.25 (d, J = 1.0 Hz, 1H). **^{13}C NMR** (101 MHz, $CDCl_3$): δ_C 27.00, 28.10, 37.72, 38.90, 79.88, 81.44, 127.92, 134.86, 165.13, 169.79, 177.23. **ESI MS:** 323.2 ($[M + Na]^+$). **HRMS (ESI):** calcd. For $C_{15}H_{24}O_6Na$ 323.14651, found: 323.14622.

4-(tert-Butyl) 1-(((Isopropoxycarbonyl)oxy)methyl) 2-Methylene-succinate (7).—Chloromethyl isopropyl carbonate (3) (393 mg, 345 μL, 2.58 mmol, 1.2 equiv); 50 °C; mobile phase: cyclohexane/EtOAc, 5:1. Compound **7** was isolated as a colorless oil (552 mg) in 85% yield. **^{1}H NMR** (401 MHz, $CDCl_3$): δ_H 6.28–6.23 (m, 1H), 5.74 (s, 2H), 5.62 (td, J = 1.2 Hz, 1H), 4.95–4.84 (m, 1H), 3.36–3.31 (m, 2H), 1.46 (s, 9H), 1.29 (d, J = 6.2 Hz, 6H). **^{13}C NMR** (101 MHz, $CDCl_3$): δ_C 169.6, 165.0, 153.4, 134.6, 128.2, 82.0, 81.5, 73.1, 37.7, 28.0, 21.7. **ESI MS:** 325.1 ($[M + Na]^+$). **HRMS** (**ESI**): calcd. for $C_{14}H_{22}O_7Na$ 325.12577; found: 325.12580.

4-(tert-Butyl) 1-(((Isopropoxycarbonyl)oxy)methyl) 2-Methylene-succinate (8).—(4-Chloromethyl)-5-methyl-1,3-dioxol-2-one (**4**) (383 mg, 282 μL, 2.58 mmol, 1.2 equiv); 55 °C; mobile phase: cyclohexane/EtOAc, 4:1. Compound **8** was isolated as a colorless oil (493 mg) in 77% yield. **^{1}H NMR** (401 MHz, $CDCl_3$): δ_H 1.46 (s, 9H), 2.16 (s, 3H), 3.31 (d, J = 0.8 Hz, 2H), 4.84 (s, 2H), 5.63 (td, J = 1.1 Hz, 1H), 6.23–6.25 (m, 1H). **^{13}C NMR** (101 MHz, $CDCl_3$): δ_C 9.49, 28.05, 37.83, 54.15, 81.48, 128.05, 133.53, 134.91, 140.30, 152.15, 165.15, 170.54. **ESI MS:** 377.0 ($[M + Na]^+$). **HRMS (ESI)**: calcd. for $C_{15}H_{14}O_{10}Na$ 377.04792; found: 377.04773.

General Synthetic Procedure for Prodrugs P4–6.

Compounds **P6–8** (1 equiv) were dissolved in anhydrous DCM (0.5–1 mL), trifluoroacetic acid (4–6 mL) was added, and the mixture was stirred for 2 h at room temperature. Volatiles were evaporated, and the residue was dissolved in DCM (3 × 15 mL) and evaporated 3 times. The residue was purified by flash column chromatography on silica (mobile phase: cyclohexane/EtOAc, 1:1) to afford desired prodrugs **P4–6.**

2-Methylene-4-oxo-4-((pivaloyloxy)methoxy)butanoic Acid (P4).—Compound **6** (140 mg, 0.466 mmol); DCM (0.5 mL), trifluoroacetic acid (4 mL). Prodrug **P4** was isolated as a colorless oil (110 mg) in 97% yield. **^{1}H NMR** (401 MHz, $CDCl_3$): δ_H 1.21 (s, 9H), 3.37 (s, 2H), 5.77 (s, 2H), 5.86 (s, 1H), 6.49 (s, 1H), 11.12 (s, 1H). **^{13}C NMR** (101 MHz, $CDCl_3$): δ_C 26.81, 36.97, 38.76, 79.66, 131.36, 132.54, 169.22, 171.11, 177.13. **ESI MS:** 267.1 ($[M + Na]^+$). **HRMS (ESI):** calcd. For $C_{11}H_{16}O_6Na$ 267.08391; found: 267.08375.

4-(((Isopropoxycarbonyl)oxy)methoxy)-2-methylene-4-oxobutanoic Acid (P5).—Compound **7** (500 mg, 1.65 mmol); DCM (1 mL), trifluoroacetic acid (6 mL). Prodrug **P5** was isolated as a colorless solid (375 mg) in 92% yield. **^{1}H NMR** (401 MHz, $CDCl_3$): δ_H 1.30 (s, 3H), 1.32 (s, 3H), 3.40 (s, 2H), 4.84–4.99 (m, 1H), 5.76 (s, 2H), 5.88 (d, J = 1.1 Hz, 1H), 6.50 (s, 1H). **^{13}C NMR** (101 MHz, $CDCl_3$): δ_C 21.75, 36.94, 73.31, 82.14, 131.72, 132.49, 153.44, 169.22, 171.37. **ESI MS:** 245.1 ($[M – H]^+$). **HRMS (ESI):** calcd. for $C_{10}H_{13}O_7$ 245.06668; found: 245.06667.

4-((5-Methyl-2-oxo-1,3-dioxol-4-yl)methoxy)-2-methylene-4-oxobutanoic Acid (P6).—Compound **8** (470 mg, 1.58 mmol); DCM (1 mL), trifluoroacetic acid (6 mL). Prodrug **P6** was isolated as a colorless solid (321 mg) in 84% yield. **^{1}H NMR** (401 MHz, $CDCl_3$): δ_H 2.19 (s, 3H), 3.40 (d, J = 1.1 Hz, 2H), 4.89 (s, 2H), 5.89 (d, J = 1.0 Hz, 1H), 6.52 (s, 1H), 11.46 (bs, 1H). **^{13}C NMR** (101 MHz, $CDCl_3$): δC 9.47, 37.17, 54.34, 131.73, 132.72, 133.43, 140.43, 152.21, 170.20, 171.42. **ESI MS:** 265.0 ($[M + Na]^+$). **HRMS (ESI):** calcd. for $C_{10}H_{10}O_7Na$ 265.03187; found: 265.03191.

Synthetic Procedure for Prodrug P7.

4-(3-(Hexadecyloxy)-propoxy)-2-methylene-4-oxobutanoic Acid (P7).—Itaconic anhydride (336 mg, 3.00 mmol, 1 equiv) and 3-(hexadecyloxy)propanol (992 mg, 3.30 mmol, 1.1 equiv) were dissolved in $CHCl_3$ (3 mL) and the mixture was stirred for 16 h at 70 °C. Volatiles were evaporated, and the residue was purified by flash column chromatography on silica (mobile phase: DCM/MeOH, 35:1) to afford 1.03 g (83%) of prodrug **P7** as a colorless solid. **^{1}H NMR** (401 MHz, $CDCl_3$): δ_H 0.88 (t, 3H, J = 6.8, 3H), 1.20–1.35 (m, 26 H), 1.60–1.51 (m, 2H), 1.89 (p, 2H), 3.34 (d, J = 1.0, 2H), 3.39 (t, J = 6.7, 2H), 3.46 (t, J = 6.2, 2H), 4.20 (t, J = 6.4, 2H), 5.83 (d, J = 1.1, 1H), 6.46 (d, J = 0.9, 1H). **^{13}C NMR** (101 MHz, $CDCl_3$): δ_C 14.28, 22.85, 26.31, 29.12, 29.52, 29.67, 29.77, 29.80, 29.82, 29.84, 29.86, 32.08, 37.47, 62.54, 67.16, 71.34, 130.79, 133.38, 170.62, 170.93. **ESI MS:** 411.3 ($[M – H]^+$). **HRMS (ESI):** calcd. for $C_{24}H_{43}O_5$ 411.31160; found: 411.31088.

General Synthetic Procedure for Prodrugs P8–10 and P11–14.

1-MI (**11**) or 4-MI (**12**) (200 mg, 1.39 mmol, 1 equiv), appropriate chloride **2–4** (1.2–1.3 equiv), sodium iodide (41.6 mg, 0.278 mmol, 0.2 equiv) and potassium carbonate (288 mg, 2.08 mmol, 1.5 equiv) were dissolved in anhydrous MeCN (5 mL) and the mixture was stirred for 16 h at 40–45 °C. EtOAc (60 mL) was added, and the mixture was washed with brine (20 mL) and sat. sodium thiosulfate (10 mL). The organic phase was dried over anhydrous Na_2SO_4, volatiles were evaporated, and the residue was purified by flash column chromatography on silica (cyclohexane/EtOAc, 5:1) to afford desired prodrugs **P8–10** and **P11–14**.

1-Methyl 4-((Pivaloyloxy)methyl) 2-Methylenesuccinate (P8).—1-MI (**11**); chloromethyl pivalate (272 mg, 260 μL, 1.80 mmol, 1.3 equiv); 40 °C. Compound **P8** was isolated as a colorless oil (301 mg) in 84% yield. **^{1}H NMR** (401 MHz, $CDCl_3$): δ_H 1.22 (s, 9H), 3.38 (s, 2H), 3.77 (s, 3H), 5.74 (dd, J = 2.1, 1.1 Hz, 1H), 5.76 (s, 2H), 6.35 (s, 1H). **^{13}C NMR** (101 MHz, $CDCl_3$): δ_C 26.95, 37.52, 38.86, 52.29, 79.75, 129.07, 133.15, 166.43, 169.51, 177.17. **ESI MS:** 281.1 ($[M + Na]^+$). **HRMS (ESI):** calcd. for $C_{12}H_{18}O_6Na$ 281.09956; found: 281.09993.

4-(((Isopropoxycarbonyl)oxy)methyl) 1-Methyl 2-Methylenesuccinate (P9).—1-MI (**11**); chloromethyl isopropyl carbonate (254 mg, 223 μL, 1.67 mmol, 1.2 equiv); 40 °C. Compound **P9** was isolated as a colorless oil (336 mg) in 93% yield. **^{1}H NMR** (401 MHz, $CDCl_3$): δ_H 1.31 (s, 3H), 1.32 (s, 3H), 3.40 (s, 2H), 3.76 (s, 3H), 4.86−4.97 (m, 1H), 5.78−5.71 (m, 3H), 6.36 (s, 1H). **^{13}C NMR** (101 MHz, $CDCl_3$): δ_C 21.65, 37.33, 52.20, 73.12, 81.96, 129.18, 132.88, 153.31, 166.33, 169.27. **ESI MS:** 283.1 ($[M + Na]^+$). **HRMS (ESI):** calcd. for $C_{11}H_{16}O_7Na$ 283.07882; found: 283.07925.

1-Methyl 4-((5-Methyl-2-oxo-1,3-dioxol-4-yl)methyl) 2-Methylenesuccinate (P10).—1-MI (**11**); (4-chloromethyl)-5-methyl-1,3-dioxol-2-one (268 mg, 197 μL, 1.80 mmol, 1.3 equiv); 40 °C. Compound **P10** was isolated as a colorless oil (298 mg) in 84% yield. **^{1}H NMR** (401 MHz, $CDCl_3$): δ_H 2.16 (s, 3H), 3.36 (s, 2H), 3.76 (s, 3H), 4.85 (s, 2H), 5.74 (d, J = 1.1 Hz, 1H), 6.35 (s, 1H). **^{13}C NMR** (101 MHz, $CDCl_3$): δ_C 9.49, 37.60, 52.35, 54.25, 129.25, 133.20, 133.43, 140.34, 152.19, 166.50, 170.33. **ESI MS:** 279.0 ($[M + Na]^+$). **HRMS (ESI):** calcd. for $C_{11}H_{12}O_7Na$ 279.04752; found: 279.04800.

4-Methyl 1-((Pivaloyloxy)methyl) 2-Methylenesuccinate (P12).—4-MI (**12**); chloromethyl pivalate (272 mg, 260 μL, 1.80 mmol, 1.3 equiv); 40 °C. Compound **P12** was isolated as a colorless oil (330 mg) in 92% yield. **^{1}H NMR** (401 MHz, $CDCl_3$): δ_H 1.20 (s, 9H), 3.34 (s, 2H), 3.68 (s, 3H), 5.79 (d, J = 1.1 Hz, 1H), 5.82 (s, 2H), 6.39 (s, 1H). **^{13}C NMR** (101 MHz, $CDCl_3$): δ_C 26.95, 37.38, 38.90, 52.21, 79.91, 130.30, 133.06, 164.82, 170.90, 177.19. **ESI MS:** 281.1 ($[M + Na]^+$). **HRMS (ESI):** calcd. for $C_{12}H_{18}O_6Na$ 281.09956; found: 281.09921.

1-(((Isopropoxycarbonyl)oxy)methyl) 4-Methyl 2-Methylenesuccinate (P13).—4-MI (**12**); chloromethyl isopropyl carbonate (254 mg, 223 μL, 1.67 mmol, 1.2 equiv); 45 °C. Compound **P13** was isolated as a colorless oil (340 mg) in a 94% yield. **^{1}H NMR** (401

MHz, $CDCl_3$): δ_H 1.33 (s, 3H), 1.34 (s, 3H), 3.38 (s, 2H), 3.72 (s, 3H), 4.86−5.02 (m, 1H), 5.82−5.88 (m, 3H), 6.46 (s, 1H). **^{13}C NMR** (101 MHz, $CDCl_3$): δ_C 21.64, 37.20, 52.12, 73.10, 82.20, 130.50, 132.76, 153.29, 164.52, 170.77. **ESI MS:** 283.1 ($[M + Na]^+$). **HRMS (ESI):** calcd. for $C_{11}H_{16}O_7Na$ 283.07882; found: 283.07855.

4-Methyl 1-((5-Methyl-2-oxo-1,3-dioxol-4-yl)methyl) 2-Methylenesuccinate (P14).—4-MI (**12**); (4-chloromethyl)-5-methyl-1,3-dioxol2-one (268 mg, 197 μL, 1.80 mmol, 1.3 equiv); 40 °C. Compound **P14** was isolated as a light-yellow oil (320 mg) in 90% yield. **^{1}H NMR** (401 MHz, $CDCl_3$): δ_H 2.17 (s, 3H), 3.33 (s, 2H), 3.67 (s, 3H), 4.91 (s, 2H), 5.78 (d, J = 1.1 Hz, 1H), 6.35 (s, 1H). **^{13}C NMR** (101 MHz, $CDCl_3$): δ_C 9.36, 37.36, 52.13, 54.28, 129.98, 132.99, 133.36, 140.30, 152.11, 165.51, 170.91. **ESI MS:** 279.1 ($[M + Na]^+$). **HRMS (ESI):** calcd. For $C_{11}H_{12}O_7Na$ 279.04752; found: 279.04757.

General Synthetic Procedure for Prodrugs P11 and P15.

1-MI (**11**) or 4-MI (**12**) (400 mg, 2.78 mmol, 1 equiv) were dissolved in anhydrous DCM (8 mL), 3-(hexadecyloxy)propanol (959 mg, 3.19 mmol, 1.15 equiv) and DMAP (509 mg, 4.16 mmol, 1.5 equiv) was added and the solution was cooled to 0 °C and stirred under inert atmosphere. A solution of DCC (859 mg, 4.16 mmol, 1.5 equiv) in anhydrous DCM (5 mL) was added dropwise for 10 min, and the resulting mixture was stirred for 1 h at 0 °C and then overnight (15 h) at room temperature. The mixture was filtered, DCM (30 mL) was added, and the organic phase was washed with 10% $KHSO_4$ (3 × 10 mL), sat. $NaHCO_3$ (10 mL) and brine (10 mL). The organic phase was dried over anhydrous Na_2SO_4, volatiles were evaporated, and the residue was purified by flash column chromatography on silica (mobile phase: cyclohexane/EtOAc, 80:15) to afford prodrugs **P11** and **P15**.

4-(3-(Hexadecyloxy)propyl) 1-Methyl 2-Methylenesuccinate (P11).—1-MI (**11**). Compound **P11** was isolated as a colorless amorphous compound (332 mg) in 28% yield. **^{1}H NMR** (401 MHz, $CDCl_3$): δ_H 0.87 (t, J = 7.0 Hz, 3H), 1.23−1.33 (m, 26 H), 1.50−1.58 (m, 2H), 1.84−1.92 (p, 2H), 3.33 (d, J = 1.2 Hz, 2H), 3.38 (t, J = 6.7 Hz, 2H), 3.45 (t, J = 6.3 Hz, 2H), 3.76 (s, 3H), 4.19 (t, J = 6.5 Hz, 2H), 5.69−5.71 (m, 1H), 6.32 (d, J = 1.1 Hz, 1H). **^{13}C NMR** (101 MHz, $CDCl_3$): δ_C 14.27, 22.84, 26.30, 29.14, 29.51, 29.66, 29.76, 29.78, 29.80, 29.82, 29.84, 29.86, 32.07, 37.89, 52.26, 62.43, 67.16, 71.32, 128.59, 128.73, 133.88, 166.79, 170.79. **ESI MS:** 449.3 ($[M + Na]^+$). **HRMS (ESI):** calcd. for $C_{25}H_{46}O_5Na$ 449.32375; found: 449.32382.

1-(3-(Hexadecyloxy)propyl) 4-Methyl 2-Methylenesuccinate (P15).—4-MI (**12**). Compound **P15** was isolated as a colorless amorphous compound (805 mg) in 68% yield. **^{1}H NMR** (401 MHz, $CDCl_3$): δ_H 0.88 (t, J = 7.0 Hz, 3H), 1.21−1.34 (m, 26 H), 1.50−1.60 (m, 2H), 1.89−1.97 (p, 2H), 3.34 (d, J = 1.2 Hz, 2H), 3.39 (t, J = 6.7 Hz, 2H), 3.48 (t, J = 6.3 Hz, 2H), 3.70 (s, 3H), 4.26 (t, J = 6.5 Hz, 2H), 5.69−5.71 (m, 1H), 6.31−6.35 (m, 1H). **^{13}C NMR** (101 MHz, $CDCl_3$): δ_C 14.26, 22.84, 26.32, 29.22, 29.51, 29.66, 29.76, 29.78, 29.81, 29.82, 29.85, 29.87, 32.08, 37.69, 52.17, 62.58, 67.23, 71.36, 128.53, 134.04, 166.20, 171.27. **ESI MS:** 427.3 ($[M + H]^+$). **HRMS (ESI):** calcd. for $C_{25}H_{47}O_5$ 427.34180; found: 427.34158.

CHEMICAL AND METABOLIC STABILITY

For measuring chemical stability, prodrugs were spiked (10 μM) in pH buffers (pH 1.2, 4.5, and 7.4) in triplicate. These mixtures were incubated at 37 °C for 1 h. Prodrug disappearance was monitored using the developed LC–MS/MS methods described below.

For measuring metabolic stability, prodrugs (10 μM) were spiked in mouse and human plasma and incubated in an orbital shaker at 37 °C. Aliquots (100 μL) were sampled at predetermined times (0 and 60 min) and quenched with cold acetonitrile (300 μL) containing internal standard (losartan 0.5 μM). The samples were vortexed for 30 s and centrifuged at 14,000*g* for 10 min. The supernatant (50 μL) was diluted with water (50 μL) and transferred to a 250 μL polypropylene vial sealed with a Teflon cap. These samples were run using liquid chromatography and high-resolution mass spectrometry (LCMS), and the disappearance of prodrugs was noted over the stipulated time. Briefly, prodrugs were analyzed on a Thermo Scientific Dionex Ultimate 3000 UPLC system coupled to Dionex Ultimate 3000 pump and autosampler using EclipsePlus C18 UPLC column from Agilent [Santa Clara, CA] (100 mm × 2.1 mm id, 1.8 μm). The autosampler was maintained at 4 °C and the column compartment at 35 °C for the duration of the LC-MS runs. Chromatographic separation was achieved using acetonitrile/water containing 0.1% formic acid as a mobile phase while pumping a flow of 0.3 mL/min for 9 min using gradient elution. The eluent was analyzed using a Thermo Scientific Q Exactive Focus mass spectrometer, equipped with a heated electrospray ionization (HESI) probe set in the positive ionization mode. Samples were introduced into the ionization source through a heated nebulized probe (350 °C). Disappearance of prodrugs was measured from the ratio of peak areas of analyte to IS.

PAMPA-GIT.

To assess intestinal permeability, we utilized STIRWELL PAMPA sandwiches (pION INC). A 5 μL of GIT-0 lipid solution was applied to coat each well of the top (acceptor) compartment of STIRWELL PAMPA sandwich. Before assembling the sandwich, the bottom (donor) plate was loaded with 200 μL of test compounds and reference compounds (10 μM) dissolved in the pION buffer at pH 7.4, containing 0.2% DMSO. The acceptor plate was filled with 200 μL of pH 7.4 sink buffer. The sandwich was incubated at room temperature for 4 h. Following the incubation, 50 μL of samples were collected from both donor and acceptor compartments and analyzed by LC-MS/MS. P_e value is calculated using the following equation.

$$P_e = -\frac{2.303 V_D}{A(t-\tau_{SS})} \cdot \log\left[1-\left(\frac{1}{1-R}\right)\frac{C_D(t)}{C_D(0)}\right]$$

where P_e is the effective permeability coefficient (cm/s), A is the filter area (0.3 cm^2) multiplied by a nominal porosity of 70% according to the manufacturer, V_D and V_A are the volumes in the donor and acceptor phase, t is the incubation time, τ_{SS} is the steady state time (s), $C_D(t)$ is the concentration (mol cm^{-3}) of the compound in the donor phase at time t, $C_D(0)$ is the concentration (mol cm^{-3}) of the compound in the donor phase at time 0, and R is the membrane retention factor

$$R = 1 - \frac{C_D(t)}{C_D(0)} - \frac{V_A}{V_D} \cdot \frac{C_A(t)}{C_D(0)}$$

NHEK Cytotoxicity.

Normal human epidermal keratinocytes (Lonza, Basel, Switzerland) were revived, allowed to expand, and seeded in 96-well plates. **P2, P9** and **P13** were diluted to concentrations of 100, 30, 10, and 1 μM and added to the assay plates containing NHEKs. The plates were checked for compound effects after 8 h of incubation to determine % viability of NHEKs. Cell viability was measured with CellTiter-Glo assay (Promega, Madison, WI).

Poly(I:C)/IFNγ-Induced Gene Expression Profiles in NHEKs.

NHEKs were seeded in plates and incubated overnight at 37 °C and 5% CO, followed by stimulation of Poly(I:C) (50 μg/mL) and IFNγ (5 ng/mL) with or without the presence of prodrugs at the concentrations of 1, 10, 30, and 100 μM. After incubation, RNA was isolated and analyzed with TaqMan RT-PCR (Thermo Fisher Scientific, Waltham, MA) to quantify fold changes in the expression of genes of IL-6, IFNβ, IL-1β, CXCL-9, CXCL-10, and CXCL-11.

Pharmacokinetic Studies.

All animal studies were conducted in accordance with protocols reviewed and approved by the Institutional Animal Care and Use Committee of Johns Hopkins University (JHU). C57BL6 mice weighing between 25–30 g and 8.5 weeks of age were maintained on a 12 h light-dark cycle, with access to food and water, ad libitum.

For PK studies, **P2** or **P13** were formulated in 10% DMSO, 80% PEG, 10% HBS v/v/v and administered PO at a dose of 100 mg/kg equivalent to either IA or MMI. All of the formulations were freshly prepared prior to the dosing. The mice were sacrificed at specified time points (0.25, 0.5, 1, 2, 4, 6, and 24 h) post drug administration. Blood samples were collected in heparinized microtubes by cardiac puncture and spun at 2000× g for 15 min to collect plasma and then 100 μL plasma was stabilized by the addition of 50 μL 2% formic acid in water and immediately frozen and stored at −80 °C.

Skin was dissected, flash frozen in liquid nitrogen, then weighed. Four microliters of 0.1% FA in 30:70 water:ACN/mg tissue was added as stabilizer. Samples were stored at −80 °C.

For quantifying intact **P2** or **P13**, IA, and 4-MI in plasma, naive mouse plasma was combined 2:1 with 2% formic acid stabilizer, aliquoted, and standard and QC stock solutions of each analyte were spiked to obtain standards (0.01–1000 nmol/mL), and QCs (0.05–500 nmol/mL). These then were protein precipitated using methanol (5 × plasma volume) containing internal standards (0.5 μM Losartan: Millipore Sigma, Burlington MA; 10 μM itaconic acid-C[13]5, Cambridge isotope libraries, Tewksbury, MA; 10 μM 5-methoxy-2-methylene-5-oxopentanoic acid (MMOPA), Enamine; Monmouth Jct., NJ.) Samples were prepared in a similar fashion (without spiking standard stock solutions) to match the ratio of matrix to solvent achieved in standards and QCs. The solutions were centrifuged at 16,000

g for 5 min at 4 °C, and the supernatant was analyzed using LC-MS/MS to quantify **P2** or **P13**, IA and 4-MI using the bioanalytical methods described below.

For quantifying intact **P2** or **P13**, IA, and 4-MI in the skin, naive skin was homogenized, and protein precipitated simultaneously using methanol (5 × tissue weight) containing internal standards in a Geno grinder at 1500 rpm for 3 min. This matrix was aliquoted, and standard and QC stock solutions of each analyte were spiked to obtain standards (0.01–1000 nmol/g), and QCs (0.05–500 nmol/g). Samples were prepared in a similar fashion (without spiking standard stock solutions) to match the ratio of matrix to solvent achieved in standards and QCs. These were then centrifuged at 16,000*g* for 5 min at 4 °C, and the supernatant was analyzed using LC-MS/MS to quantify the analytes using the bioanalytical methods described below.

Bioanalysis.

Chromatographic analysis was performed using an Ultimate 3000 ultrahigh-performance system consisting of coupled with a QExactive Focus orbitrap mass spectrometer (Thermo Fisher Scientific Inc., Waltham, MA). Analyte separation was achieved at 35 °C using an Agilent EclipsePlus column (100 mm × 2.1 mm i.d.) packed with 1.8 μm C18 stationary phase. The mobile phase consisted of 0.1% formic acid in methanol and 0.1% formic acid in water with gradient elution. The $[M + H]^+$ ion transition for **P2** was m/z 363.1286 → 105.0592 and 113.0291 with losartan as internal standard. The $[M + H]^+$ transition for losartan were m/z 423.1695 → 207.0915 and 377.1518. The $[M + H]^+$ ion transition for **P13** was m/z 261.0969 → 69.0339, 99.0474, and 127.0386 with losartan as internal standard as above. The $[M - H]^-$ ion transition for IA was m/z 129.0193 → 85.0294 with IA-[13C]5 as internal standard. The $[M - H]^-$ ion transition for IA-[13C]5 was m/z 134.0361 → 89.0429. The $[M + H]^+$ ion transition for 4-MI was m/z 145.0495 → 69.0339 and 99.0474 with MMOPA as internal. standard The $[M + H]^+$ transition for MMOPA were m/z 159.0652 → 113.0656 and 127.0388.

Supplementary Material

Refer to Web version on PubMed Central for supplementary material.

ACKNOWLEDGMENTS

The synthetic part of this work was supported by a grant from Ministry of Education, Youths and Sports of the Czech Republic (LM2023053, program EATRIS-CZ).

ABBREVIATIONS USED

ACN	Acetonitrile
DCM	dichloromethane
DMI	dimethyl itaconate
EtOAc	ethyl acetate
4-EI	4-ethyl itaconate

HDP	3-(hexadecyloxy)propyl
HPLC	high-performance liquid chromatography
HRMS	high-resolution mass spectrometry
IRG1	immune-responsive gene 1
POC	isopropoxycarbonyloxymethyl
IA	itaconic acid
1-MI	1-methyl itaconate
4-MI	4-methyl itaconate
NMR	(5-methyl-2-oxo-1,3-dioxol-4-yl)methyl (ODOL);nuclear magnetic resonance
NHEK	normal human epidermal keratinocyte
4-OI	4-octyl itaconate
PAMPA	parallel artificial membrane permeability assay
POM	pivaloyloxymethyl
NaI	sodium iodide
SDH	succinate dehydrogenase
TCA	tricarboxylic acid

REFERENCES

(1). O'Neill LAJ; Artyomov MN Itaconate: the poster child of metabolic reprogramming in macrophage function. Nat. Rev. Immunol 2019, 19 (5), 273–281. [PubMed: 30705422]

(2). Ferreira AV; Netea MG; Dominguez-Andres J. Itaconate as an immune modulator. Aging 2019, 11 (12), 3898–3899. [PubMed: 31235675]

(3). Lampropoulou V; Sergushichev A; Bambouskova M; Nair S; Vincent EE; Loginicheva E; Cervantes-Barragan L; Ma X; Huang SC; Griss T; et al. Itaconate Links Inhibition of Succinate Dehydrogenase with Macrophage Metabolic Remodeling and Regulation of Inflammation. Cell Metab. 2016, 24 (1), 158–166. [PubMed: 27374498]

(4). Lawrence GW; Ovsepian SV; Wang J; Aoki KR; Dolly JO Extravesicular intraneuronal migration of internalized botulinum neurotoxins without detectable inhibition of distal neurotransmission. Biochem. J 2012, 441 (1), 443−452. [PubMed: 21929507]

(5). Qin W; Qin K; Zhang Y; Jia W; Chen Y; Cheng B; Peng L; Chen N; Liu Y; Zhou W; et al. S-glycosylation-based cysteine profiling reveals regulation of glycolysis by itaconate. Nat. Chem. Biol 2019, 15 (10), 983–991. [PubMed: 31332308]

(6). Song H; Xu T; Feng X; Lai Y; Yang Y; Zheng H; He X; Wei G; Liao W; Liao Y; et al. Itaconate prevents abdominal aortic aneurysm formation through inhibiting inflammation via activation of Nrf2. EBioMedicine 2020, 57, No. 102832.

(7). Bambouskova M; Gorvel L; Lampropoulou V; Sergushichev A; Loginicheva E; Johnson K; Korenfeld D; Mathyer ME; Kim H; Huang LH; et al. Electrophilic properties of itaconate and

derivatives regulate the IkappaBzeta-ATF3 inflammatory axis. Nature 2018, 556 (7702), 501–504. [PubMed: 29670287]

(8). Swain A; Bambouskova M; Kim H; Andhey PS; Duncan D; Auclair K; Chubukov V; Simons DM; Roddy TP; Stewart KM; Artyomov MN Comparative evaluation of itaconate and its derivatives reveals divergent inflammasome and type I interferon regulation in macrophages. Nat. Metab 2020, 2 (7), 594–602. [PubMed: 32694786]

(9). Hooftman A; Angiari S; Hester S; Corcoran SE; Runtsch MC; Ling C; Ruzek MC; Slivka PF; McGettrick AF; Banahan K; et al. The Immunomodulatory Metabolite Itaconate Modifies NLRP3 and Inhibits Inflammasome Activation. Cell Metab. 2020, 32 (3), 468–478.e7. [PubMed: 32791101]

(10). Runtsch MC; Angiari S; Hooftman A; Wadhwa R; Zhang Y; Zheng Y; Spina JS; Ruzek MC; Argiriadi MA; McGettrick AF; et al. Itaconate and itaconate derivatives target JAK1 to suppress alternative activation of macrophages. Cell Metab. 2022, 34 (3), 487–501.e8. [PubMed: 35235776]

(11). Yang S; Zhang X; Zhang H; Lin X; Chen X; Zhang Y; Lin X; Huang L; Zhuge Q. Dimethyl itaconate inhibits LPS-induced microglia inflammation and inflammasome-mediated pyroptosis via inducing autophagy and regulating the Nrf-2/HO-1 signaling pathway. Mol. Med. Rep 2021, 24 (3), No. 672, DOI: 10.3892/mmr.2021.12311.

(12). Li W; Li Y; Kang J; Jiang H; Gong W; Chen L; Wu C; Liu M; Wu X; Zhao Y; Ren J. 4-octyl itaconate as a metabolite derivative inhibits inflammation via alkylation of STING. Cell Rep. 2023, 42 (3), No. 112145.

(13). ElAzzouny M; Tom CT; Evans CR; Olson LL; Tanga MJ; Gallagher KA; Martin BR; Burant CF Dimethyl Itaconate Is Not Metabolized into Itaconate Intracellularly. J. Biol. Chem 2017, 292 (12), 4766–4769. [PubMed: 28188288]

(14). Hooftman A; O'Neill LAJ The Immunomodulatory Potential of the Metabolite Itaconate. Trends Immunol. 2019, 40 (8), 687–698. [PubMed: 31178405]

(15). Lin J; Ren J; Gao DS; Dai Y; Yu L. The Emerging Application of Itaconate: Promising Molecular Targets and Therapeutic Opportunities. Front. Chem 2021, 9, No. 669308.

(16). Tsai J; Gori S; Alt J; Tiwari S; Iyer J; Talwar R; Hinsu D; Ahirwar K; Mohanty S; Khunt C; et al. Topical SCD-153, a 4-methyl itaconate prodrug, for the treatment of alopecia areata. PNAS Nexus 2023, 2 (1), No. pgac297.

(17). Hecker SJ; Erion MD Prodrugs of phosphates and phosphonates. J. Med. Chem 2008, 51 (8), 2328–2345. [PubMed: 18237108]

(18). Babu KS; Reddy MS; Tagore AR; Reddy GS; Sebastian S; Varma MS; Venkateswarlu G; Bhattacharya A; Reddy PP; Anand RV Efficient synthesis of olmesartan medoxomil, an antihypertensive drug. Synth. Commun 2008, 39 (2), 291–298.

(19). Garaga S; Misra NC; Reddy AVR; Prabahar KJ; Takshinamoorthy C; Sanasi PD; Babu KR Commercial synthesis of Azilsartan Kamedoxomil: An angiotensin II receptor blocker. Org. Process Res. Dev 2015, 19 (4), 514–519.

(20). Hostetler KY Alkoxyalkyl prodrugs of acyclic nucleoside phosphonates enhance oral antiviral activity and reduce toxicity: current state of the art. Antiviral Res. 2009, 82 (2), A84–98. [PubMed: 19425198]

(21). Pradere U; Garnier-Amblard EC; Coats SJ; Amblard F; Schinazi RF Synthesis of nucleoside phosphate and phosphonate prodrugs. Chem. Rev 2014, 114 (18), 9154–9218. [PubMed: 25144792]

(22). Dash RP; Tichy T; Veeravalli V; Lam J; Alt J; Wu Y; Tenora L; Majer P; Slusher BS; Rais R. Enhanced Oral Bioavailability of 2-(Phosphonomethyl)-pentanedioic Acid (2-PMPA) from its (5-Methyl-2-oxo-1,3-dioxol-4-yl)methyl (ODOL)-Based Prodrugs. Mol. Pharmaceutics 2019, 16 (10), 4292–4301.

(23). Majer P; Jancarik A; Krecmerova M; Tichy T; Tenora L; Wozniak K; Wu Y; Pommier E; Ferraris D; Rais R; Slusher BS Discovery of Orally Available Prodrugs of the Glutamate Carboxypeptidase II (GCPII) Inhibitor 2-Phosphonomethylpentanedioic Acid (2-PMPA). J. Med. Chem 2016, 59 (6), 2810–2819. [PubMed: 26930119]

(24). Chollet AM; Le Diguarher T; Kucharczyk N; Loynel A; Bertrand M; Tucker G; Guilbaud N; Burbridge M; Pastoureau P; Fradin A; et al. Solid-phase synthesis of alpha-substituted 3-bisarylthio N-hydroxy propionamides as specific MMP inhibitors. Bioorg. Med. Chem 2002, 10 (3), 531–544. [PubMed: 11814839]

(25). Faller B. Artificial membrane assays to assess permeability. Curr. Drug Metab 2008, 9 (9), 886–892. [PubMed: 18991585]

(26). Daina A; Michielin O; Zoete V. SwissADME: a free web tool to evaluate pharmacokinetics, drug-likeness and medicinal chemistry friendliness of small molecules. Sci. Rep 2017, 7, No. 42717.

(27). Wils P; Warnery A; Phung-Ba V; Legrain S; Scherman D. High lipophilicity decreases drug transport across intestinal epithelial cells. J. Pharmacol. Exp. Ther 1994, 269 (2), 654–658. [PubMed: 8182532]

(28). Kawaguchi N; Ebihara T; Takeuchi T; Morohashi A; Yamasaki H; Tagawa Y; Takahashi J; Kondo T; Asahi S. Absorption of TAK-491, a new angiotensin II receptor antagonist, in animals. Xenobiotica 2013, 43 (2), 182–192. [PubMed: 22867273]

(29). Schurek KN; Wiebe R; Karlowsky JA; Rubinstein E; Hoban DJ; Zhanel GG Faropenem: review of a new oral penem. Expert Rev. Anti-Infect. Ther 2007, 5 (2), 185–198. [PubMed: 17402834]

(30). Tsaioun K; Blaauboer BJ; Hartung T. Evidence-based absorption, distribution, metabolism, excretion (ADME) and its interplay with alternative toxicity methods. ALTEX 2016, 33 (4), 343–358. [PubMed: 27806179]

(31). Heidel KM; Dowd CS Phosphonate prodrugs: an overview and recent advances. Future Med. Chem 2019, 11 (13), 1625–1643. [PubMed: 31469328]

(32). Shin JM; Choi DK; Sohn KC; Kim SY; Min Ha J; Ho Lee Y; Im M; Seo YJ; Deok Kim C; Lee JH; et al. Double-stranded RNA induces inflammation via the NF-kappaB pathway and inflammasome activation in the outer root sheath cells of hair follicles. Sci. Rep 2017, 7, No. 44127.

(33). Shin JM; Choi DK; Sohn KC; Koh JW; Lee YH; Seo YJ; Kim CD; Lee JH; Lee Y. Induction of alopecia areata in C3H/HeJ mice using polyinosinic-polycytidylic acid (poly[I:C]) and interferon-gamma. Sci. Rep 2018, 8 (1), No. 12518.

(34). Xing L; Dai Z; Jabbari A; Cerise JE; Higgins CA; Gong W; de Jong A; Harel S; DeStefano GM; Rothman L; et al. Alopecia areata is driven by cytotoxic T lymphocytes and is reversed by JAK inhibition. Nat. Med 2014, 20 (9), 1043–1049. [PubMed: 25129481]

(35). Pratt CH; King LE Jr.; Messenger AG; Christiano AM; Sundberg JP Alopecia areata. Nat. Rev. Dis Primers 2017, 3, No. 17011.

(36). Glickman JW; Dubin C; Renert-Yuval Y; Dahabreh D; Kimmel GW; Auyeung K; Estrada YD; Singer G; Krueger JG; Pavel AB; Guttman-Yassky E. Cross-sectional study of blood biomarkers of patients with moderate to severe alopecia areata reveals systemic immune and cardiovascular biomarker dysregulation. J. Am. Acad. Dermatol 2021, 84 (2), 370–380. [PubMed: 32376430]

(37). McPhee CG; Duncan FJ; Silva KA; King LE Jr.; Hogenesch H; Roopenian DC; Everts HB; Sundberg JP Increased expression of Cxcr3 and its ligands, Cxcl9 and Cxcl10, during the development of alopecia areata in the mouse. J. Invest. Dermatol 2012, 132 (6), 1736–1738. [PubMed: 22358057]

(38). Hoffmann R. The potential role of cytokines and T cells in alopecia areata. J. Invest. Dermatol. Symp. Proc 1999, 4 (3), 235–238.

(39). Hoffmann R; Eicheler W; Wenzel E; Happle R. Interleukin-1beta-induced inhibition of hair growth in vitro is mediated by cyclic AMP. J. Invest. Dermatol 1997, 108 (1), 40–42. [PubMed: 8980284]

(40). Hoffmann R; Eicheler W; Huth A; Wenzel E; Happle R. Cytokines and growth factors influence hair growth in vitro. Possible implications for the pathogenesis and treatment of alopecia areata. Arch. Dermatol. Res 1996, 288 (3), 153–156. [PubMed: 8967784]

(41). Hoffmann R; Wenzel E; Huth A; van der Steen P; Schaufele M; Henninger HP; Happle R. Cytokine mRNA levels in Alopecia areata before and after treatment with the contact allergen diphenylcyclopropenone. J. Invest. Dermatol 1994, 103 (4), 530–533. [PubMed: 7930677]

(42). Fetter T; de Graaf DM; Claus I; Wenzel J. Aberrant inflammasome activation as a driving force of human autoimmune skin disease. Front. Immunol 2023, 14, No. 1190388.

(43). Chen LL; Morcelle C; Cheng ZL; Chen X; Xu Y; Gao Y; Song J; Li Z; Smith MD; Shi M; et al. Itaconate inhibits TET DNA dioxygenases to dampen inflammatory responses. Nat. Cell Biol 2022, 24 (3), 353–363. [PubMed: 35256775]

(44). Xie QM; Chen N; Song SM; Zhao CC; Ruan Y; Sha JF; Liu Q; Jiang XQ; Fei GH; Wu HM Itaconate Suppresses the Activation of Mitochondrial NLRP3 Inflammasome and Oxidative Stress in Allergic Airway Inflammation. Antioxidants 2023, 12 (2), No. 489.

(45). Aso K; Kono M; Kanda M; Kudo Y; Sakiyama K; Hisada R; Karino K; Ueda Y; Nakazawa D; Fujieda Y; et al. Itaconate ameliorates autoimmunity by modulating T cell imbalance via metabolic and epigenetic reprogramming. Nat. Commun 2023, 14 (1), No. 984.

(46). Mills EL; Ryan DG; Prag HA; Dikovskaya D; Menon D; Zaslona Z; Jedrychowski MP; Costa ASH; Higgins M; Hams E; et al. Itaconate is an anti-inflammatory metabolite that activates Nrf2 via alkylation of KEAP1. Nature 2018, 556 (7699), 113–117. [PubMed: 29590092]

(47). McGettrick AF; Bourner LA; Dorsey FC; O'Neill LAJ Metabolic Messengers: itaconate. Nat. Metab 2024, 6 (9), 1661–1667. [PubMed: 39060560]

(48). Hoisnard L; Lebrun-Vignes B; Maury S; Mahevas M; El Karoui K; Roy L; Zarour A; Michel M; Cohen JL; Amiot A; et al. Adverse events associated with JAK inhibitors in 126,815 reports from the WHO pharmacovigilance database. Sci. Rep 2022, 12 (1), No. 7140.

(49). Mori S; Ogata F; Tsunoda R. Risk of venous thromboembolism associated with Janus kinase inhibitors for rheumatoid arthritis: case presentation and literature review. Clin. Rheumatol 2021, 40 (11), 4457–4471. [PubMed: 34554329]

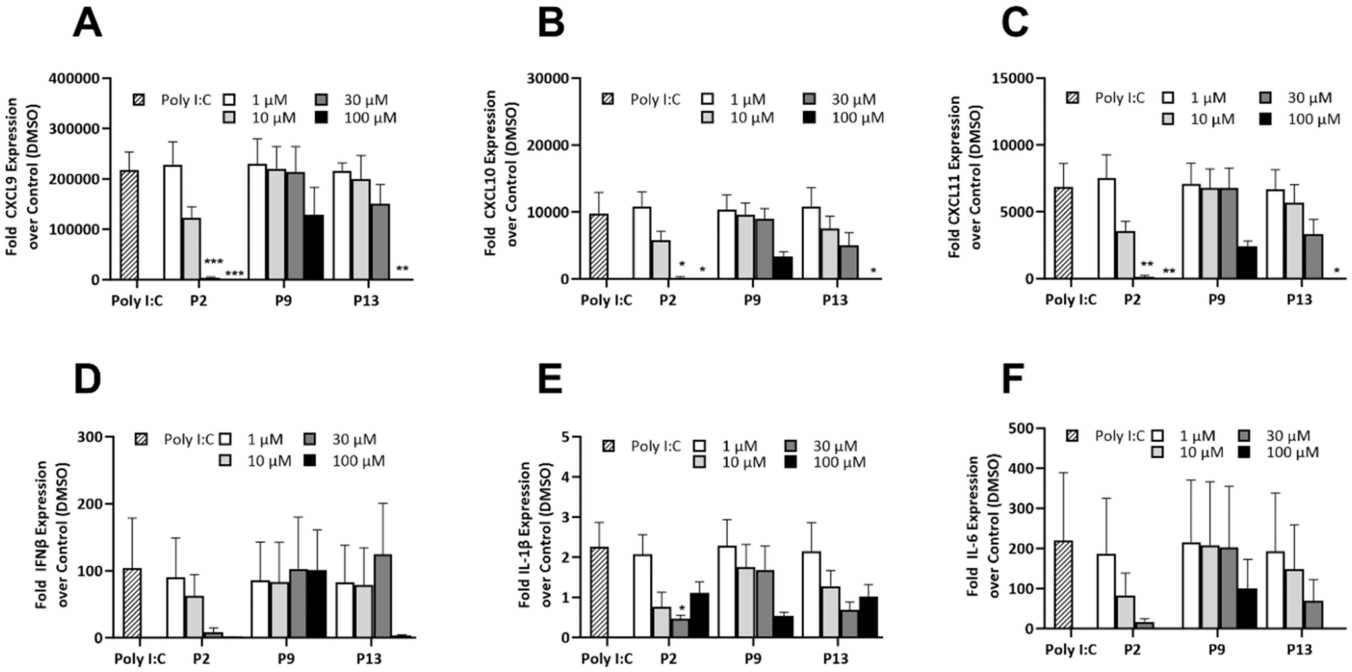

Figure 1.

Effect of **P2, P9** and **P13** on gene expression in Poly(I:C) + IFNγ stimulated NHEK cells. Induction of the chemokine and cytokine genes in primary human keratinocyte cells was measured at 8 h following incubation of **P2, P9** and **P13** (1–100 μM) as follows: CXCL 9 (A), CXCL 10 (B), CXCL 11 (C), IFNβ (D), IL-1β (E), and IL-6 (F). Poly(I:C) (50 μg/mL) + IFNγ (5 ng/mL) was used as the stimulant. Data expressed as mean ± SEM, $n = 3$. Statistical analysis was performed using one-way ANOVA by Dunnett's multiple comparisons test with comparing with Poly(I:C) + IFNγ alone; ***$p < 0.0005$, **$p < 0.005$; *$p < 0.05$.

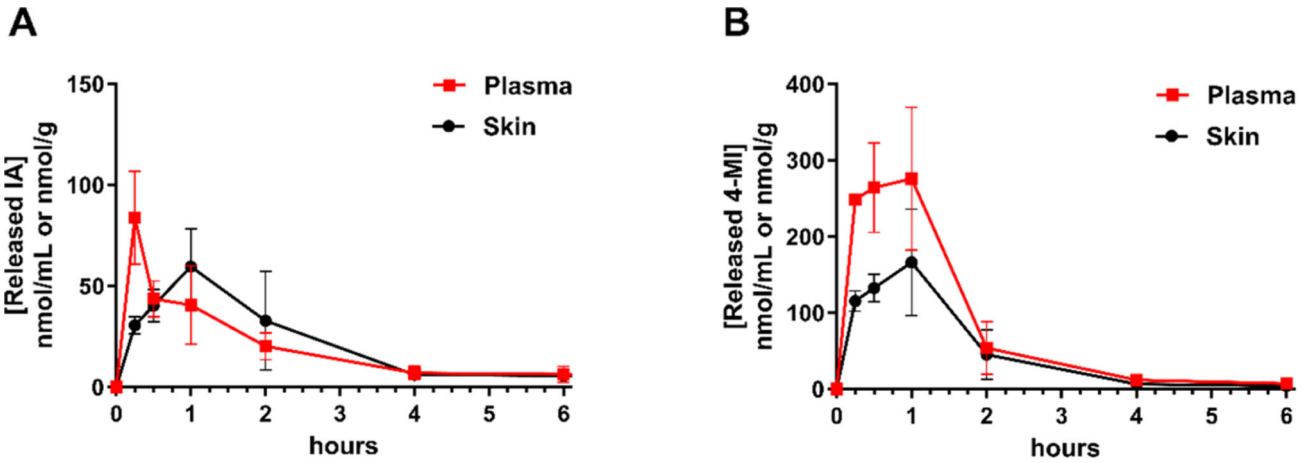

C

Treatment	Dose (mg/kg)	Analyte	Tissue	C_{max} (μM or nmol/g)	T_{max} (hr)	AUC_{0-t} (μM*h or nmol*h /g)	$T_{1/2}$ (h)	Skin/Plasma ratio
P2	100 mg/kg equivalent	IA	Plasma	83.8 ± 18.8	0.25	108 ± 2.68	1.42 ± 0.28	1.61 ± 0.29
			Skin	65.9 ± 10.2	1	173 ± 30.0	3.32 ± 1.23	
P13	100 mg/kg equivalent	4-MI	Plasma	349 ± 39.3	0.5	415 ± 16.8	0.80 ± 0.09	0.59 ± 0.01
			Skin	192 ± 38.5	1	234 ± 1.30	0.97 ± 0.20	

Figure 2.

Delivery of IA or 4-MI in plasma and skin of mice dosed with **P2** and **P13**, respectively. (A), release of IA in mice dosed with **P2** (B), release of 4-MI in mice dosed with **P13**, and (C), PK parameters of IA released from **P2**, and 4-MI released from **P13** with data expressed as means ± SEM (n = 3 per time point).

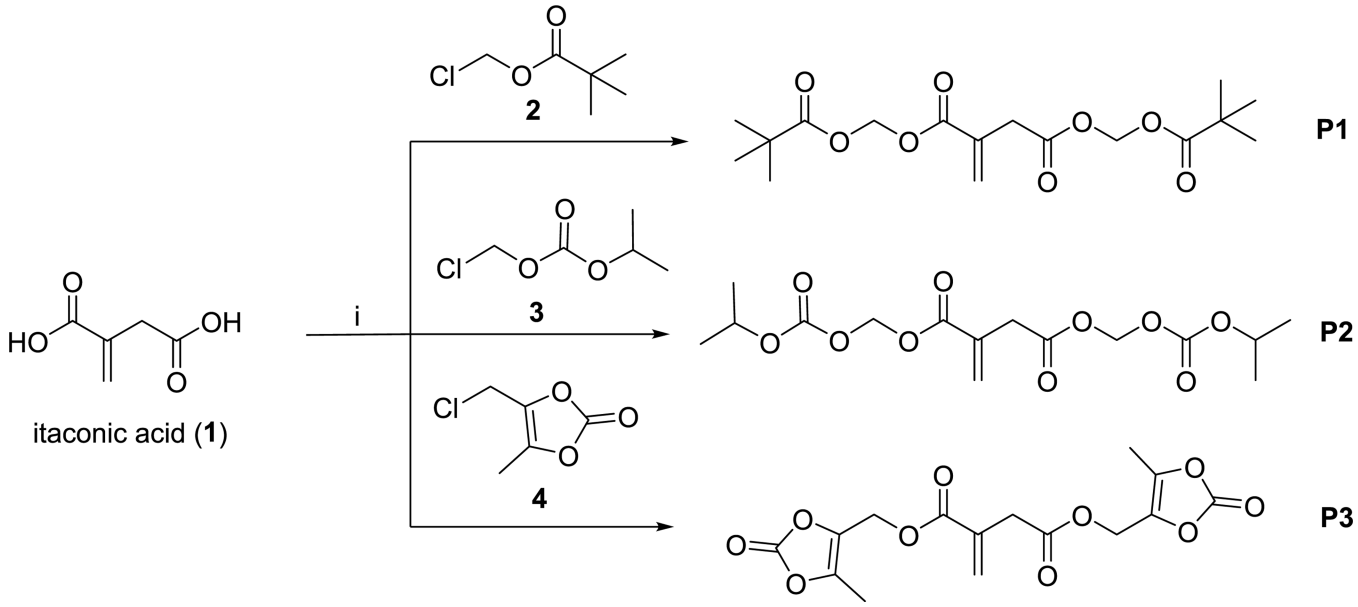

Scheme 1. Synthesis of Bis-POM, Bis-POC and Bis-ODOL Dialkyl Esters P1–3[a]

[a]Reagents and conditions: (i) K_2CO_3, NaI, MeCN, 40–55 °C, 16 h, 14–57%.

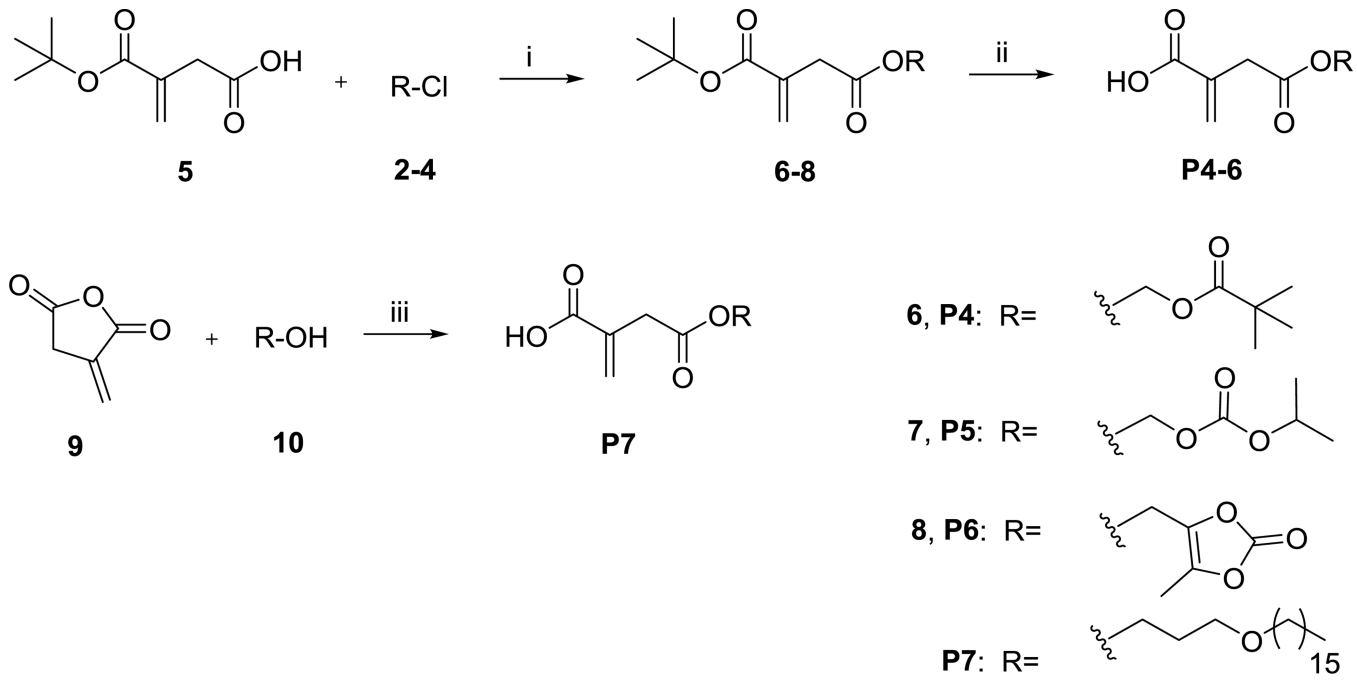

Scheme 2. Synthesis of POM, POC, ODOL, and HDP Itaconic Monoesters P4–6 and P7[a]

[a]Reagents and conditions: (i) K_2CO_3, NaI, MeCN, 40–55 °C, 16 h, 71–85%; (ii) trifluoroacetic acid in DCM, rt, 2 h, 84–97%; (iii) $CHCl_3$, 70 °C, 16 h, 83%.

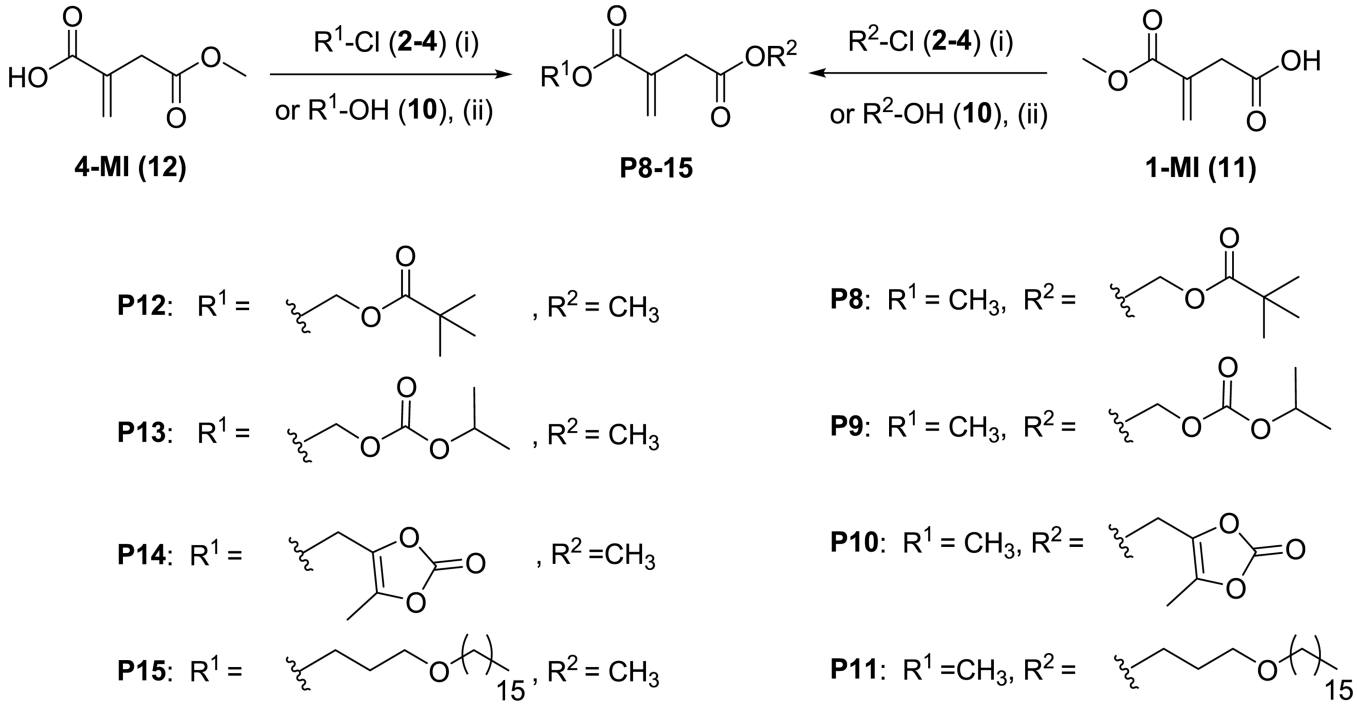

Scheme 3. Synthesis of Itaconate Diesters Designed to Release 1-MI or 4-MI[a]

[a]Reagents and conditions: (i) K_2CO_3, NaI, MeCN, 40–45 °C, 16 h, 84–94%; (ii) DCC, DMAP, 0 °C to rt, 16 h, 28–68%.

Table 1.

Structure, Stability, and Permeability of Itaconate Prodrugs

Compound ID	Molecular Structure (Blue=active moiety; Red=promoiety)	ClogP	Chemical Stability (% remaining at 1h)			Permeability (P_e, $\times 10^{-6}$ cm/sec) pH 7.4	Metabolic Stability (% remaining at 1h)			
			pH 1.2	pH 4.5	pH 7.4		Mouse Plasma	Mouse Skin	Human Plasma	Human Skin
P1	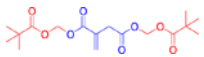	2.74	106 ± 9	92 ± 3	104 ± 17	35.8	0 ± 0	0 ± 0	0 ± 0	0 ± 0
P4	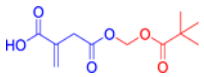	1.27	100 ± 2	74 ± 3	22 ± 4	0.08	3 ± 1	14 ± 0.5	83 ± 2	40 ± 0.7
P8	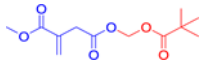	1.79	101 ± 2	104 ± 5	86 ± 8	35.2	0 ± 0	0 ± 0	0 ± 0	9.4 ± 0.9
P12	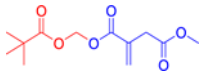	1.61	99 ± 2	109 ± 4	94 ± 1	33.2	0 ± 0	5.3 ± 0.4	0 ± 0	15 ± 2.9
P2	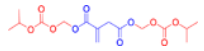	1.83	104 ± 2	109 ± 6	47 ± 4	35.9	0 ± 0	2.5 ± 2.4	0 ± 0	1.1 ± 0.4
P5	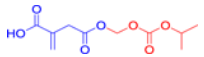	0.82	104 ± 0	79 ± 11	44 ± 1	0	0 ± 0	4.9 ± 1.3	53 ± 1	29 ± 0.9
P9	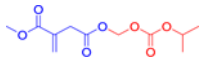	1.34	98 ± 2	94 ± 2	63 ± 3	29.3	0 ± 0	0 ± 0	0 ± 0	0 ± 0
P13	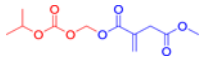	1.16	108 ± 1	103 ± 4	102 ± 2	35.3	0 ± 0	0 ± 0	0 ± 0	1.6 ± 0.4
P3	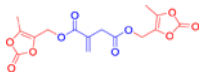	−0.94	102 ± 1	91 ± 2	91 ± 14	17.0	0 ± 0	0 ± 0	0 ± 0	30 ± 0.4
P6	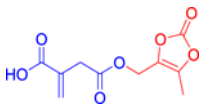	−0.66	109 ± 4	88 ± 1	0 ± 0	0	20 ± 8	74 ± 30	0 ± 0	93 ± 4

J Med Chem. Author manuscript; available in PMC 2025 April 14.

Compound ID	Molecular Structure (Blue=active moiety; Red=promoiety)	ClogP	Chemical Stability (% remaining at 1h)			Permeability (P_e, $\times 10^{-6}$ cm/sec) pH 7.4	Metabolic Stability (% remaining at 1h)			
			pH 1.2	pH 4.5	pH 7.4		Mouse Plasma	Mouse Skin	Human Plasma	Human Skin
P10	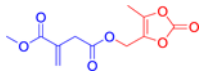	−0.13	100 ± 6	97 ± 4	69 ± 5	16.3	0 ± 0	0 ± 0	0 ± 0	56 ± 0.9
P14	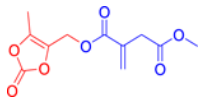	−0.14	98 ± 3	87 ± 6	99 ± 4	15.4	0 ± 0	16 ± 0.4	0 ± 0	76 ± 4
P7	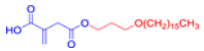	8.38	91 ± 2	90 ± 10	65 ± 4	3.2	92 ± 8	100 ± 9.5	68 ± 9	87 ± 7
P11	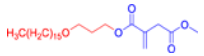	8.79	109 ± 14	98 ± 4	97 ± 4	0	89 ± 2	61 ± 10	90 ± 4	101 ± 8
P15	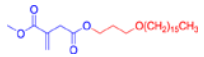	8.91	103 ± 12	108 ± 16	75 ± 8	0	44 ± 10	67 ± 11	32 ± 2	94 ± 5
IA	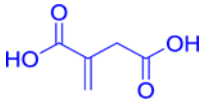	−0.33				0	-		-	
4-MI	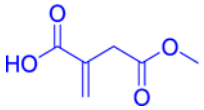	0.14				0	-		-	
1-MI	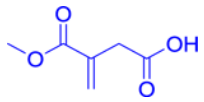	0.20				0	-		-	

J Med Chem. Author manuscript; available in PMC 2025 April 14.